International Geology Review, Vol. 44, 2002, p. 653–669.
Copyright © 2002 by V. H. Winston & Son, Inc. All rights reserved.

Tectonic Evolution of the West Kunlun: Geochronologic and Geochemical Constraints from Kudi Granitoids

CHAO YUAN,

Guangzhou Institute of Geochemistry, Chinese Academy of Sciences, Guangzhou 510640, China and Department of Earth Sciences, The University of Hong Kong, Pokfulam Road, Hong Kong, China

MIN SUN,[1] MEI-FU ZHOU,

Department of Earth Sciences, The University of Hong Kong, Pokfulam Road, Hong Kong, China

HUI ZHOU,

Department of Geology, Peking University, Beijing, 100871, China

WEN-JIAO XIAO, AND JI-LIANG LI

Institute of Geology and Geophysics, Chinese Academy of Sciences, Beijing, 100029, China

Abstract

The West Kunlun contains important information about the early evolutionary history of the Tibetan Plateau. Single-grain zircon U-Pb dating and systematic geochemical analyses were conducted on representative granitic plutons from the Kudi area. The earliest Paleozoic magmatism (471 ± 5 Ma) possesses characteristics of volcanic-arc granites, indicating that Proto-Tethys started to close in the Mid-Ordovician. An arc-continent collision occurred in the Late Ordovician, corresponding to the closure of Proto-Tethys. Following the collision, extensional deformation began in the Early Devonian and gave rise to a post-dynamic, A-type North Kudi Pluton (405 ± 2 Ma) and coeval lamprophyre dikes. Extension was pervasive throughout the whole Kunlun orogenic belt, and was responsible for Devonian to Early Permian magmatic quiescence. The reoccurrence of magmatism in the West Kunlun took place in the Early Permian, when Paleo-Tethys started to be consumed, and a new subduction zone developed in the West Kunlun. Paleo-Tethys closed by the Late Triassic (214 ± 1Ma), and led to rapid uplift and voluminous post-collisional granites.

Introduction

THE TIBETAN PLATEAU is composed of several terranes of various origins, which were accreted to the southern margin of Laurasia during consumption of the Tethyan Ocean (Chang et al., 1986, 1989; Dewey et al., 1988). The Kunlun Mountain range lies along the northern margin of the Plateau, and is divided into West and East Kunlun, extending westward to the North Pamir Range of Afghanistan (Debon et al., 1987). This mountain belt resulted from subduction of Proto- and Paleo-Tethys, and records the earliest stage of plateau formation (Pan et al., 1994; Hsü et al., 1995). Preliminary studies revealed that both the West and East Kunlun orogens have similar evolutionary histories (Matte et al., 1996; Yin and Harrison, 2000). However, some geological issues are not well understood, particularly in the West Kunlun where steep topography, high elevation, and widespread glaciers make investigation difficult. Therefore it is not easy to elucidate the bewilderingly complex evolution of the West Kunlun solely by analyses of strata and tectonic facies. Metamorphism, deformation, and erosion have greatly obscured the original geologic record in this old orogenic belt.

Two contrasting tectonic models have been proposed for the evolution of the West Kunlun. One is the archipelago model of Yao and Hsü (1994) and Hsü et al. (1995), which envisages the West Kunlun as a magmatic arc resulting from continuous consumption of Tethys (*sensu lato*) since the Late Precambrian. The second model, based on geochronological data of granitic intrusions in the West Kunlun (Pan et al., 1994; Xu et al., 1994;), invokes two stages of subduction to explain magmatic quiescence during Middle Paleozoic time. However, the paucity of high-quality geochronologic

[1]Corresponding author; email: minsun@hkucc.hku.hk

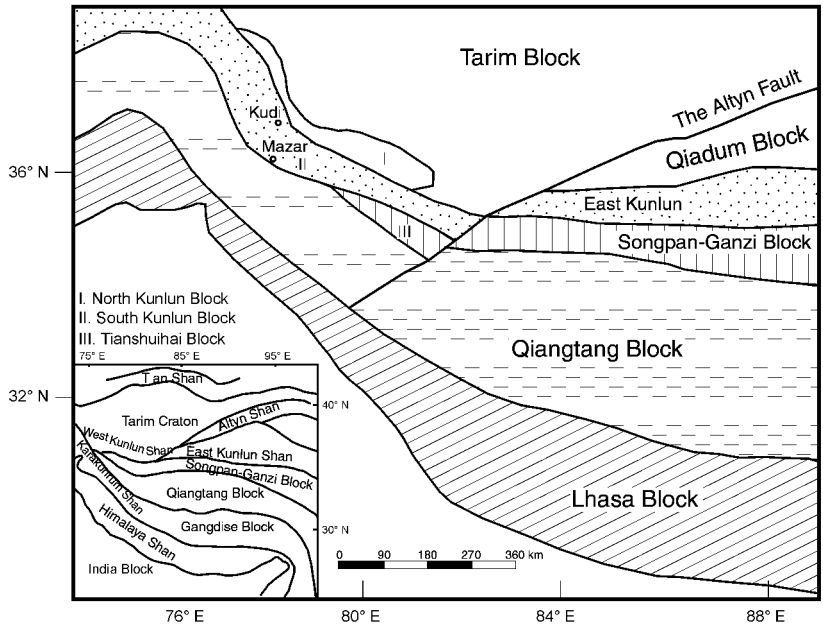

FIG. 1. Schematic map of terranes in the Tibetan Plateau.

data do not allow us to precisely constrain the timing of subduction-related magmatism, and the time of closure of Proto- and Paleo-Tethys.

Magmatic rocks in this orogenic belt may provide necessary constraints on tectonic evolution (Sengör et al., 1991, 1993), because their compositions characteristically reflect tectonic settings, their ages are related to orogenic events, and they are more resistant to erosion than metamorphic and sedimentary rocks (Pitcher, 1993; Pearce et al., 1984; Barbarin, 1999). Here we present new zircon U-Pb isotope results and geochemical data for three representative granitic plutons from the West Kunlun. These granitoids cover more than half of the Kudi area. The new data, interpreted in combination with field evidence, provide a coherent picture for the Paleozoic–Early Mesozoic evolution of the West Kunlun.

Regional Geology

The West Kunlun is divided into North and South Kunlun blocks by the Kudi suture (Fig. 1) (Pan et al., 1994; Matte et al., 1996), which is marked by the Kudi ophiolite made up of ultramafic rocks, basalts, flysch sediments, and turbidites (Deng, 1995; Yang et al., 1996; Wang et al., 2000). The age of this ophiolite is constrained by radiolarian fossils recently discovered in the flysch sediments, suggesting deposition in the Early Paleozoic (Fang et al., 1998; Zhou et al., 1998). The North Kunlun Block is in fault contact with the Tarim craton in the north and the South Kunlun Block is bounded by the Karakash strike-slip fault in the south (Matte et al., 1996), which is coincident with the suture of Paleo-Tethys (Pan et al., 1994) (Fig. 1).

The basement of the North Kunlun Block is dominated by gneissic and migmatitic rocks, cut by a 2.2 Ga granitic intrusion (Pan, 1994; Xu et al., 1994). A 2.8 Ga Nd depleted-mantle model age was reported for the gneissic rock, suggesting that this block probably had an Archean basement similar to that of the Tarim craton (Arnaud and Vidal, 1990). The overlying sedimentary cover is composed of clastic rocks and carbonates, including the Sinian to Ordovician Kilian Group (Chang et al., 1989), the Devonian Tisnab Group (XBGMR, 1985), and a sequence of Late Paleozoic to Cenozoic strata (Pan and Bian, 1996; Mattern et al., 1996).

The South Kunlun Block consists of a metamorphic complex primarily composed of schist and gneiss with local, lens-shaped ultramafic rocks (Gaetani et al., 1990; Deng, 1995). The overlying strata are dominated by Upper Paleozoic to Meso-

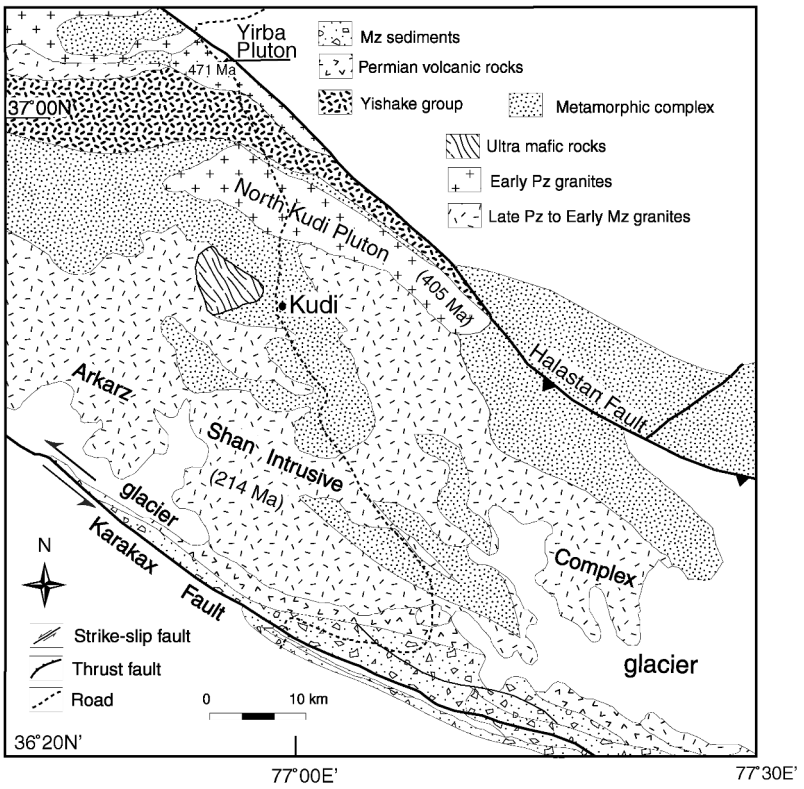

FIG. 2. Geological map of the Kudi area, West Kunlun.

zoic clastic rocks, carbonates, and calc-alkaline volcanic rocks (GITT, 1985; Pan et al., 1994; Wang, 1996) (Fig. 2). Although this metamorphic complex is lithologically similar to the basement of the North Kunlun Block, its age is not well constrained. Isotope data for the gneissic complex of the South Kunlun Block and the associated granitic intrusions both give Nd depleted-mantle model ages of 1.1 to 1.5 Ga (Zhou, 1998; Yuan, 1999), suggesting that this block has a much younger basement (Yuan et al., 2002). $^{40}Ar/^{39}Ar$ dates for the hornblende, biotite, and K-feldspar separates from the South Kunlun metamorphic complex range from 451 Ma to 350 Ma (Matte et al., 1996; Li et al., 2000; Zhou et al., 2000), which were interpreted to record an Early Paleozoic collisional event between the North and South Kunlun blocks (Matte et al., 1996).

Granitic plutons are widely exposed in the West Kunlun and exhibit a gradual southward younging trend (Wang and Fang, 1987). The following three representative granitic plutons in the Kudi area (Figs. 1 and 2) were sampled for this study.

Yirba pluton

The Yirba pluton is located about 20 km north of Kudi. It intrudes the South Kunlun metamorphic complex in the west and is truncated by the Halastan fault in the east (Fig. 2). This pluton is composed of medium- to coarse-grained plagioclase (55%), K-feldspar (15%), quartz (20%), and subordinate hornblende and biotite. Accessory minerals include magnetite, sphene, zircon, and apatite. The pluton is deformed, with well-developed lineation and foliation defined by hornblende and biotite, consistent with the NW/SE shearing in the country rocks (Mattern et al., 1996). Previous geological investigations suggested that the pluton intruded the volcanic sequence of the Kudi ophiolite (i.e., Yishake Group) along its southern margin (Pan et al., 1994; Matte et al., 1996). However, more recent field work casts doubt on the intrusive relationship

and has identified a fault contact between the pluton and the Yishake volcanic sequence (Mattern and Schneider, 2000; Xiao et al., 2002). Previous geochronological studies have not provided consistent data for this pluton. Conventional zircon U-Pb analysis yielded $1912^{+53}/_{-52}$ Ma and $458^{+2.4}/_{-2.5}$ Ma upper and lower intercept ages, respectively, whereas single-grain zircon evaporation provided Pb-Pb ages of 480 to 510 Ma (Li et al., 1995). Hornblende and biotite separates gave $^{40}Ar/^{39}Ar$ plateau ages of 476 ± 9 and 496 ± 4 Ma, respectively (Xu et al., 1994).

North Kudi pluton (NKP)

The NKP intruded the metamorphic complex of the South Kunlun Block (Fig. 2). This pluton has a monzogranite composition, with medium-grained K-feldspar (>50%), plagioclase (<10%), quartz (~25%), and biotite (10%). Accessory minerals (5%) include sphene, apatite, zircon, monazite, and magnetite. The pluton is undeformed and has a typical granitic texture. It truncates the fabrics of the metamorphic country rocks, showing that intrusion followed the regional metamorphism/deformation, i.e., was post-kinematic (Matte et al., 1996). Previous conventional U-Pb zircon dating yielded a U-Pb age of $384^{+2}/_{-1}$ Ma, (Xu et al., 1994), whereas biotite separates gave similar or slightly older $^{40}Ar/^{39}Ar$ ages (397 to 381 Ma) (Arnaud, 1992; Xu et al., 1994; Zhang et al., 1998).

Arkarz Shan intrusive complex (ASIC)

The voluminous ASIC is exposed mainly along the crest of the West Kunlun (Fig. 2), covering an area of more than 2,800 km^2. It consists of undeformed fine- to medium-grained granodiorite and biotite monzogranite, intruding the metamorphic complex and the lower Permian arc volcanic rocks of the South Kunlun Block (Fig.2). Samples have similar mineral assemblages, including plagioclase (30–35%), K-feldspar (15–35%), quartz (25–40%), biotite (~15%), and rare hornblende. Accessory minerals include zircon, apatite, sphene, allanite, monazite, zoisite, and magnetite. K-feldspar and biotite separates from the ASIC yielded $^{40}Ar/^{39}Ar$ ages of 180 ± 10 Ma and 221± 6.6 Ma, respectively (Xu et al., 1992, 1994). No zircon U-Pb data were previously available.

Analytical Methods

After crushing, the sample chips were cleaned with deionized water in an ultrasonic vessel, dried, and then ground into powder (<200 mesh) in an agate mill. Zircon crystals were separated using conventional heavy liquid techniques, and then handpicked under the microscope. U and Pb were separated using cation-exchange technique (AG1 × 8, 200–400 resin), following the procedure of Li et al. (1995). U-Pb isotope measurements were conducted on a VG-354 thermal ionization mass spectrometer (TIMS) in the Tianjing Institute of Geology and Mineral Resources. The total Pb blank of the whole procedure was less than 0.05 ng, and the U blank was less than 0.004 ng. Common lead was corrected using the model of Stacey and Kramers (1975), and isotopic data were processed using the ISOPLOT program of Ludwig (1998).

Major-element analyses were performed on a Rigaku® RIX 2000 XRF spectrometer on glass discs in the Department of Geology, National University of Taiwan, following the procedure of Goto and Tatsumi (1996). Trace-element data were analyzed, employing the sinter fusion-ICPMS method. The $Li_2B_4O_7$ fused beads were digested with mixed acid ($HF + HNO_3$). Pure solution external standards were used for calibration and geostandards (USGS standards G-2, SY-4, and W-2, and Chinese National Standards GSR-1 and GSR-3) were analyzed to monitor the quality of the analyses (Liu et al., 1996). Measurements were performed on a VG Elemental® PQ3 ICP-MS at the University of Hong Kong. Precisions for REEs were better than 5%, whereas the precisions for Rb, Sr, Cs, Ba, Nb, Zr, Hf, Ta, U, and Th were better than 10%.

Results

Zircon U-Pb geochronology

Zircons analyzed in this study are colorless or brownish-yellow, generally smaller than 0.5 mm, and free of visible cores, cracks, and inclusions. The results are presented in Table 1.

Five zircon crystals from the Yirba Pluton contain intermediate U (600–1000 ppm) and high Pb (60–80 ppm) contents, all lying on or close to the concordia (Fig. 3A). These zircons apparently fall into two age groups, i.e., 491 ± 3 Ma and 471 ± 5 Ma, respectively.

Five zircon crystals from the NKP have relatively low U (300–700 ppm) and intermediate Pb (25–60

TABLE 1. Zircon U-Pb Isotopic Data of the Representative Granitic Plutons of the Kudi Area[1]

Sample no.	Color	Weight μg	U μg/g	Pb μg/g	Pb_{com} ng	$^{206}Pb/^{204}Pb$	$^{208}Pb/^{206}Pb$	$^{206}Pb/^{238}U$	$^{207}Pb/^{235}U$	$^{207}Pb/^{206}Pb$	$^{206}Pb/^{238}U$, Ma	$^{207}Pb/^{235}U$, Ma	$^{207}Pb/^{206}Pb$ Ma
						Yirba pluton							
96-KL-158-1	Light yellow	15	817	70	0.079	784	0.1086	0.07916(59)	0.6133(92)	0.05619(71)	491.1	485.6	460.0
96-KL-158-2	Light yellow	10	956	79	0.022	2155	0.1226	0.07909(75)	0.6187(84)	0.05674(49)	490.7	489.0	481.4
96-KL-158-3	Light yellow	15	670	74	0.350	156	0.08871	0.07681(64)	0.6113(88)	0.05772(62)	477.1	484.4	519.0
96-KL-158-4	Light yellow	10	807	65	0.033	1189	0.1037	0.07599(89)	0.6035(100)	0.05759(60)	472.2	479.4	514.4
96-KL-158-5	Light brown	15	633	57	0.120	380	0.1140	0.07601(73)	0.5922(83)	0.05651(52)	472.2	472.3	472.4
						North Kudi pluton							
96-KL-196-1	Brown	30	629	53	0.350	236	0.1318	0.06468(65)	0.4896(60)	0.05490(35)	404.0	404.6	408.1
96-KL-196-2	Colorless	30	389	31	0.140	351	0.1661	0.06469(80)	0.4897(79)	0.05491(51)	404.1	404.7	408.5
96-KL-196-3	Light purplish red	15	634	56	0.180	231	0.1907	0.06459(70)	0.4896(83)	0.05497(65)	403.5	404.6	411.1
96-KL-196-4	Light purplish red	20	345	25	0.018	1581	0.1804	0.06510(104)	0.4919(113)	0.05481(81)	406.6	406.2	404.3
96-KL-196-5	Light purplish red	20	719	53	0.110	558	0.1258	0.06511(49)	0.4931(54)	0.05493(39)	406.6	407.0	409.5
						Akarz Shan Intrusive Complex							
						Monzogranite							
96-KL-211-1	Brown	30	1589	57	0.042	2452	0.1343	0.03411(33)	0.2374(26)	0.05048(24)	216.2	216.3	217.1
96-KL-211-2	Colorless	30	1084	39	0.049	1434	0.1334	0.03363(35)	0.2341(30)	0.05048(33)	213.3	213.6	217.3
96-KL-211-3	Light purplish red	20	996	50	0.310	158	0.1457	0.03392(33)	0.2356(37)	0.05037(56)	215.0	214.8	212.1
96-KL-211-4	Light purplish red	20	1289	46	0.037	1488	0.1351	0.03379(28)	0.2351(29)	0.05046(42)	214.2	214.4	216.4
Granodiorite													
96-KL-62-1	Light purplish red	15	922	36	0.076	406	0.1291	0.03348(51)	0.2327(55)	0.05042(83)	212.3	212.5	214.5
96-KL-62-2	Light purplish red	15	841	36	0.120	244	0.1330	0.03344(54)	0.2326(59)	0.05045(90)	212.0	212.3	215.8
96-KL-62-3	Light purplish red	15	733	29	0.064	383	0.09990	0.03349(63)	0.2335(68)	0.05057(103)	212.3	213.1	221.4
96-KL-62-4	Light purplish red	10	729	33	0.087	195	0.1013	0.03330(90)	0.2313(99)	0.05037(152)	211.2	211.2	212.1
96-KL-62-5	Light yellow	10	888	35	0.068	283	0.1251	0.03183(76)	0.2204(89)	0.05022(150)	202.0	202.2	205.0

[1] $^{206}Pb/^{204}Pb$ values have been corrected for laboratory blank (Pb = 0.050 ng, U = 0.002 ng; $^{206}Pb/^{204}Pb = 17.97 \pm 1$, $^{207}Pb/^{204}Pb = 15.55 \pm 0.5$, $^{208}Pb/^{204}Pb = 37.706 \pm 1.5$) and spike ($^{206}Pb/^{205}Pb = 0.052765$, $^{206}Pb/^{204}Pb = 185.14$, $^{206}Pb/^{207}Pb = 15.4$, $^{206}Pb/^{208}Pb = 6.3063$). Pb isotopes in other isotope ratios are all radiogenic. Data in brackets represent 2 sigma errors.

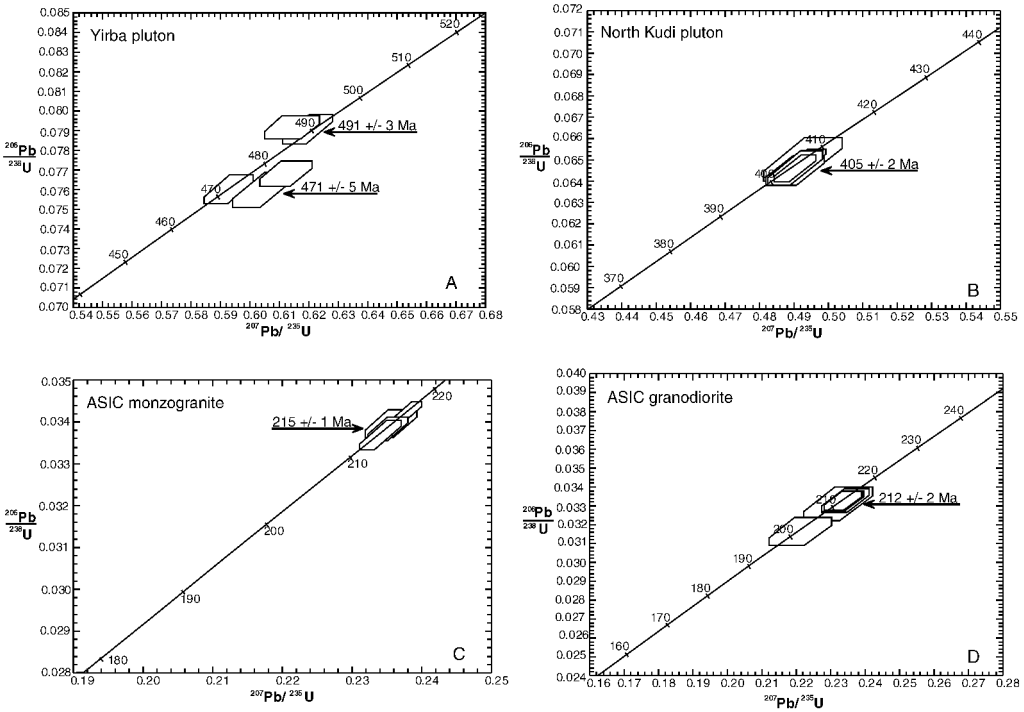

FIG. 3. Concordia diagrams for granitoids of the Kudi area.

ppm) contents. All of these zircons are concordant, giving an age of 405 ± 2 Ma (Table 1, Fig. 3B).

Four zircon grains from the ASIC monzogranite have U and Pb concentrations ranging from 1000 to 1600 ppm, and 40 to 60 ppm, respectively, and give a concordant age of 215 ± 1 Ma (Fig. 3C). Five zircons from the ASIC granodiorite possess lower U (700–1000 ppm) and Pb (30–40 ppm) contents, but yield a similar concordant age of 212 ± 2 Ma (Table 1, Fig. 3D).

Major- and trace-element geochemistry

Major-element compositions and nomenclature of the granites in this study are presented in Table 2 and Figure 4. In general, the granitic rocks are metaluminous, with ACNK values less than 1.1 (Table 2). The Yirba pluton contains relatively low SiO_2 (55–62 wt%) and high $Fe_2O_3^*$ (6.0–8.1 wt%), MgO (2.2–3.3 wt%), and CaO contents (3.8–6.8 wt%). Most samples plot in the quartz monzodiorite and granodiorite fields (Fig. 4A), and show I-type granite affinity (Fig. 4B). The rocks exhibit LREE-enriched patterns ($(La/Yb)_N$ = 15–23), with minor negative Eu anomalies (δEu= 0.7–0.8) (Fig. 5A), and are relatively enriched in LILE and depleted in HFSE, as indicated by low Nb/La (0.3–0.4) and Rb/Nb (6–10) ratios.

The NKP has a uniform monzogranitic composition (Fig. 4A), with intermediate SiO_2 (67–71 wt%) and high K_2O contents (K_2O > 5.5 wt%) (Table 2). Samples from this pluton possess relatively high REE (346–501 ppm) and display LREE-enriched patterns ($(La/Yb)_N$ = 8.4–19) with intermediate negative Eu anomalies (δEu = 0.5–0.6) (Fig. 5B). These samples are HFSE enriched, as evidenced by high Zr, Nb, and Y contents and relatively high Nb/La (0.5–1.0) and low Rb/Nb (3.5–5.2) ratios, exhibiting a strong affinity to A-type granites (Fig. 4B).

The ASIC possesses a wide range of SiO_2 contents (54~73 wt%) and can be subdivided into two groups, according to their SiO_2 and alkali contents. Samples with relatively high SiO_2 (>70 wt%) are generally K_2O rich and cluster in the monzogranite field. The low-SiO_2 group (<70 wt%) includes both relatively Na_2O-rich and K_2O-rich samples and ranges from granodiorite to monzogranite, with an average composition of granodiorite (Table 2, Fig. 4A). Both groups show LREE-enriched patterns

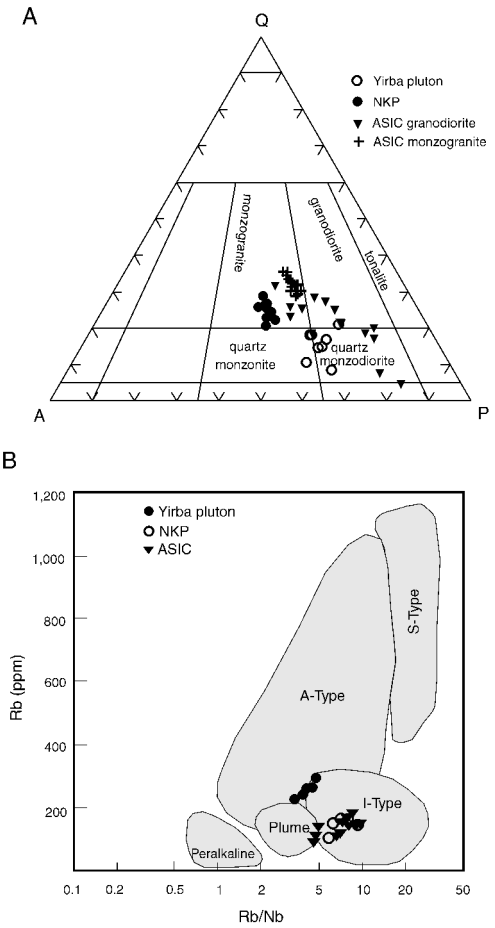

FIG. 4. A. Classification for granitoids of the Kudi area (after Le Maitre, 1989). Abbreviations: Q = quartz; A = alkali feldspar, P = plagioclase. CIPW normative mineral proportions were used for plotting. B. Rb/Nb versus Rb diagram for the granitoids from the Kudi area (after Christansen and Keith, 1996)

$((La/Yb)_N$ = 6–28) with intermediate negative Eu anomalies (δEu = 0.5–0.8) (Figs. 5C and 5D), and are characterized by relatively low Nb/La (0.3–0.6) and high Rb/Nb (5–12) ratios. The ASIC rocks plot in the I-type granite field (Fig. 4B).

Discussion: Ages and Tectonic Settings of the Granitoids

Yirba pluton

Inasmuch as there is no evidence for multiple magmatic injections for this small pluton, the younger age (471 ± 5 Ma) is interpreted to represent the crystallization age of the Yirba pluton, whereas the older age (491 ± 3 Ma) is considered to be inherited from the magma source. The regional deformation in the study area was ascribed to the collision between the North and South Kunlun blocks, after the closure of Proto-Tethys in the Middle Paleozoic (Matte et al., 1996; Mattern et al., 1996; Pan, 1996). The regional lineation/foliation crosscuts the Yirba pluton, indicating that the pluton was formed prior to the collisional event (Wang and Fang, 1987). The 471 Ma Early Ordovician age further supports this interpretation. In the tectonic discrimination diagram of Pearce et al. (1984), samples mainly fall in the VAG field (Fig. 6), implying a subduction-related setting. Chemical compositions show affinity to adakites (Wang et al., 2000), which are commonly produced by partial melting of subducted oceanic lithosphere beneath island arcs (Defant and Drummond, 1990). However, relatively radiogenic Sr isotopic compositions (initial $^{87}Sr/^{86}Sr$ = 0.7073–0.7089) (Yuan, 1999) do not favor this comparison. Fault contact with the Yishake volcanic sequence, which was produced in an intra-oceanic arc setting (Yuan, 1999), may imply that the Yirba pluton probably intruded in a different environment. We consider that the Yirba Pluton was generated in an active continental margin during consumption of Proto-Tethys.

North Kudi pluton

The new zircon U-Pb age (405 ± 2 Ma) is significantly older than previous conventional U-Pb zircon and biotite $^{40}Ar/^{39}Ar$ results, suggesting that the NKP was formed in the Early Devonian. The NKP was previously considered to be subduction-related, due to its calc-alkaline nature (Yao and Hsü, 1994; Li et al., 1995; Ding et al., 1996). However, detailed field studies constrain a post-collisional setting, because the regional fabrics do not pass through this pluton (Matte et al., 1996). The low Rb/Nb and high Nb/La ratios and alkali-enriched features show its affinity to A-type granites, which usually intrude in anorogenic or post-orogenic environments (Eby, 1992). Coeval lamprophyre dikes in the Kudi area, with a hornblende $^{39}Ar/^{40}Ar$ plateau age of 405 ± 3 Ma, were recently recognized (Zhou and Li, 2000), suggesting that the area was under extension in Early Devonian time. In the tectonic discrimination diagram, the NKP plots in the WPG field (Fig. 6), consistent with our post-orogenic interpretation.

TABLE 2. Major and Trace Element Compositions of Representative Granitic Plutons of the Kudi Area

Pluton:					Yirba pluton					North Kudi pluton	
Sample:	96-KL-43	96-KL-45	96-KL-48	96-KL-158	96-KL-159	96-KL-160	96-KL-161	96-KL-162	96-KL-163	96-KL-174	96-KL-176
SiO_2	61.7	56.4	58.8	60.3	59.0	58.6	60.3	54.9	58.8	70.7	71.2
TiO_2	0.74	0.75	0.56	0.59	0.59	0.62	0.49	0.74	0.55	0.44	0.47
Al_2O_3	18.4	16.6	16.4	16.5	16.2	16.5	15.7	16.8	16.6	14.6	14.7
Fe_2O_3*	6.92	7.52	7.39	6.17	6.93	6.55	6.03	8.09	6.34	2.01	2.08
MnO	0.15	0.13	0.14	0.10	0.13	0.12	0.12	0.15	0.11	0.07	0.08
MgO	2.35	3.30	2.94	2.28	2.79	2.40	2.24	2.96	2.44	0.28	0.37
CaO	3.78	5.11	5.88	4.74	4.33	5.68	5.15	6.81	5.69	0.80	1.15
Na_2O	4.20	2.83	2.57	2.81	3.31	3.06	3.00	3.12	2.93	3.62	3.60
K_2O	1.32	4.47	2.84	4.12	3.99	3.80	4.00	3.65	3.56	5.99	5.66
P_2O_5	0.21	0.48	0.18	0.36	0.37	0.38	0.34	0.47	0.36	0.09	0.11
Total	99.73	97.52	97.73	97.96	97.69	97.75	97.35	97.58	97.31	98.57	99.35
Be			1.78	4.00		3.57		4.36	3.91		5.60
Rb			107	167		151		162	146		242
Sr			470	830		811		864	854		173
Y			19.4	28.5		25.0		34.0	23.1		47.2
Zr			51.3	193		180		233	172		437
Nb			17.4	21.0		17.7		24.2	14.5		57.4
Cs			1.13	1.97		2.09		2.22	2.03		8.42
Ba			811	1444		1223		1133	1425		507
La			47.5	74.5		57.0		87.5	65.1		55.0
Ce			92.2	139		109		160	116		146
Pr			11.3	16.0		13.1		18.6	13.1		20.6
Nd			38.1	56.4		47.9		66.2	46.3		76.2
Sm			7.02	10.2		9.01		12.3	8.13		13.7
Eu			1.58	2.49		2.24		2.79	2.05		2.15
Gd			6.65	9.09		7.61		10.4	6.82		10.7
Tb			0.86	1.06		0.94		1.26	0.84		1.48
Dy			4.61	5.37		4.9		6.4	4.24		7.76
Ho			0.82	0.98		0.89		1.17	0.77		1.52
Er			2.20	2.59		2.31		2.96	2.06		4.4
Tm			0.33	0.38		0.34		0.45	0.28		0.67
Yb			2.17	2.44		2.18		2.88	1.92		4.43
Lu			0.33	0.38		0.32		0.42	0.29		0.65
Hf			2.09	5.54		5.22		6.33	4.67		11.2
Ta			1.05	1.07		1.01		1.27	0.74		3.00
Th			9.11	21.5		27.8		24.2	17.5		16.2
U			1.03	3.53		6.48		5.27	2.67		3.95

Continues

TABLE 2. Continued

Pluton:	North Kudi pluton							Arkarz Shan intrusive complex			
								Granodiorite			
Sample:	96-KL-177	96-KL-178	96-KL-179	96-KL-181	96-KL-182	96-KL-193	96-KL-196	96-KL-62	96-KL-63	96-KL-65	96-KL-66
SiO_2	69.8	68.6	68.1	70.5	71.5	67.3	68.3	67.7	53.9	57.2	68.5
TiO_2	0.61	0.62	0.57	0.43	0.43	0.76	0.65	0.25	0.84	0.60	0.25
Al_2O_3	14.8	15.0	15.4	14.2	13.8	14.9	14.5	16.2	20.0	19.5	15.4
Fe_2O_3[1]	2.70	2.67	2.52	1.93	2.06	3.36	3.02	2.79	7.83	6.12	2.57
MnO	0.09	0.09	0.08	0.08	0.08	0.09	0.08	0.06	0.16	0.12	0.05
MgO	0.47	0.49	0.51	0.28	0.34	0.73	0.61	0.40	1.80	1.21	0.37
CaO	1.32	1.32	1.18	1.16	0.92	1.86	1.67	2.18	5.55	5.35	1.96
Na_2O	3.54	3.66	3.84	3.60	3.51	3.61	3.50	3.81	4.92	4.87	3.76
K_2O	5.68	5.81	6.08	5.59	5.57	5.45	5.50	4.99	2.10	2.64	4.78
P_2O_5	0.13	0.14	0.14	0.10	0.11	0.21	0.18	0.09	0.32	0.24	0.09
Total	99.16	98.44	98.46	97.87	98.3	98.21	98.04	98.42	97.43	97.81	97.79
Be	5.80		6.41		7.28		5.72	1.3	3.82	3.15	2.46
Rb	224		263		285		243	173	103	130	193
Sr	202		204		154		217	232	430	458	256
Y	50.5		48.6		38.4		41.0	15.1	25.8	20.7	18.2
Zr	481		472		368		372	170	322	311	190
Nb	64.1		60.7		54.9		53.5	20.2	22.0	19.3	22.6
Cs	8.97		11.23		8.84		8.99	2.33	1.51	1.96	2.84
Ba	728		832		551		966	828	540	722	879
La	109		102		106		102	61.4	43.8	40.2	63.3
Ce	220		215		192		190	107	85.1	70.8	109
Pr	26.9		26.5		22.0		21.4	11.2	9.98	7.84	11.1
Nd	92.0		90.7		71.0		70.8	32.3	36.0	27.0	34.2
Sm	15.5		15.0		11.4		11.6	4.54	6.52	4.74	5.3
Eu	2.47		2.37		1.77		2.07	0.77	1.62	1.59	0.81
Gd	12.5		12.2		9.4		9.91	4.33	6.04	4.24	4.72
Tb	1.58		1.60		1.16		1.28	0.54	0.83	0.59	0.59
Dy	8.52		8.27		6.11		7.10	2.93	4.54	3.35	3.15
Ho	1.62		1.61		1.21		1.38	0.59	0.89	0.7	0.64
Er	4.74		4.64		3.47		4.17	1.75	2.55	2.09	1.92
Tm	0.70		0.72		0.55		0.64	0.29	0.36	0.37	0.3
Yb	4.76		4.57		3.79		4.3	1.83	2.42	2.81	2.21
Lu	0.68		0.67		0.58		0.61	0.34	0.38	0.47	0.32
Hf	12.0		11.9		9.39		10.6	6.51	8.36	8.65	6.33
Ta+	3.32		3.2		2.66		3.12	1.78	1.05	1.54	1.93
Th	26.9		21.6		34.9		27.4	32.0	11.9	10.4	29.2
U	5.34		4.52		6.74		6.19	4.04	2.54	3.15	3.95

Continues

TABLE 2. Continued

Pluton:	Arkarz Shan intrusive complex										
				Granodiorite				Monzogranite			
Sample	96-KL-139	96-KL-257	96-KL-260	96-KL-261	96-KL-262	96-KL-263	96-KL-264	96-KL-200	96-KL-201	96-KL-202	96-KL-203
SiO_2	65.4	60.5	69.7	61.7	61.0	62.0	71.2	71.8	72.8	71.4	70.5
TiO_2	0.66	0.66	0.28	0.60	0.71	0.69	0.25	0.17	0.18	0.20	0.22
Al_2O_3	16.7	18.5	14.8	18.2	18.4	17.3	14.6	14.2	13.6	14.9	15.1
Fe_2O_3*	5.15	6.15	2.99	5.87	6.60	6.53	2.84	2.44	2.19	2.61	2.89
MnO	0.09	0.13	0.05	0.11	0.12	0.14	0.06	0.07	0.07	0.06	0.07
MgO	0.99	1.21	0.43	1.09	1.30	1.27	0.37	0.19	0.25	0.22	0.27
CaO	3.23	4.08	1.80	4.10	3.94	3.47	1.82	1.44	1.36	1.48	1.71
Na_2O	3.18	4.67	3.13	4.57	4.44	4.01	3.40	3.89	3.40	3.76	3.94
K_2O	4.23	2.19	4.81	1.96	2.37	3.00	4.17	4.17	4.31	4.28	4.00
P_2O_5	0.20	0.21	0.10	0.19	0.23	0.22	0.09	0.07	0.07	0.07	0.08
Total	99.8	98.28	98.13	98.4	99.09	98.63	98.77	98.37	98.22	98.92	98.78
Be	2.96		3.05	3.12			4.91				2.97
Rb	151		165	128			203				131
Sr	313		244	388			185				211
Y	38.4		19.6	19.2			31.6				15.3
Zr	328		205	403			194				184
Nb	30.0		16.5	25.9			23.8				16.5
Cs	4.02		6.06	8.87			13.5				3.26
Ba	1111		1066	455			700				1500
La	71.5		60.7	79.4			39.1				60.3
Ce	136		106	137			68.4				101
Pr	15.6		11.1	14.2			7.15				10.1
Nd	53.0		33.9	45.4			22.7				30.5
Sm	9.66		5.19	6.46			3.88				4.53
Eu	1.66		0.97	1.40			0.69				0.90
Gd	8.66		4.52	5.41			3.84				3.82
Tb	1.21		0.55	0.66			0.59				0.46
Dy	6.93		3.13	3.35			4.11				2.54
Ho	1.38		0.65	0.67			0.95				0.49
Er	3.99		1.94	1.87			3.15				1.48
Tm	0.59		0.32	0.3			0.58				0.24
Yb	3.97		2.36	1.92			4.31				1.75
Lu	0.59		0.37	0.31			0.7				0.26
Hf	9.77		6.29	10.9			5.95				5.33
Ta	1.49		1.37	1.14			2.6				0.93
Th	19.4		26.8	32.4			23.5				16.8
U	2.76		3.57	2.24			3.14				1.51

Continues

TABLE 2. Continued

Pluton:	Arkarz Shan Intrusive Complex										
						Monzogranite					
Sample	96-KL-204	96-KL-207	96-KL-209	96-KL-210	96-KL-211	96-KL-239	96-KL-241	96-KL-243	96-KL-245	96-KL-267	96-KL-268
SiO_2	70.5	72.7	71.6	70.2	73.6	71.4	71.8	71.6	62.1	71.1	72.9
TiO_2	0.21	0.16	0.21	0.21	0.18	0.17	0.18	0.17	0.61	0.19	0.18
Al_2O_3	15.1	14.0	14.4	15.0	13.7	14.7	14.2	14.6	17.0	14.6	13.7
Fe_2O_3*	2.93	2.30	2.78	2.78	2.21	2.18	2.32	2.15	5.71	2.50	2.18
MnO	0.07	0.06	0.07	0.07	0.07	0.05	0.07	0.05	0.12	0.06	0.07
MgO	0.28	0.19	0.25	0.27	0.27	0.14	0.26	0.14	1.26	0.23	0.26
CaO	1.62	1.31	1.45	1.63	1.40	1.75	1.57	1.58	4.08	1.52	1.38
Na_2O	3.94	3.73	3.69	3.94	3.53	3.78	3.85	3.68	4.43	3.81	3.55
K_2O	4.21	4.26	4.20	4.31	4.17	4.01	4.07	4.15	2.38	4.40	4.27
P_2O_5	0.08	0.07	0.08	0.08	0.07	0.06	0.07	0.06	0.19	0.08	0.07
Total	98.96	98.71	98.72	98.52	99.28	98.21	98.33	98.11	97.91	98.43	98.62
Be		2.99	4.02		3.48			3.22	4.12		
Rb		167	175		169			179	178		
Sr		150	173		158			168	390		
Y		17.4	20.1		15.1			19.2	25.7		
Zr		159	191		135			174	261		
Nb		18.2	21.4		18.0			15.2	22.3		
Cs		3.91	8.13		3.31			5.9	4.5		
Ba		976	1110		870			934	1224		
La		51.4	64.5		47.9			50.8	58.0		
Ce		89.4	110		79.7			87.9	101		
Pr		9.14	11.3		7.85			8.83	10.7		
Nd		28.0	36.7		23.2			27.2	34.7		
Sm		4.26	5.01		3.47			4.33	5.84		
Eu		0.63	0.74		0.57			0.71	1.32		
Gd		3.82	4.59		3.08			3.93	5.30		
Tb		0.52	0.57		0.40			0.51	0.73		
Dy		2.88	3.16		2.37			2.89	4.27		
Ho		0.61	0.64		0.49			0.63	0.87		
Er		1.76	1.89		1.58			1.89	2.52		
Tm		0.3	0.31		0.25			0.31	0.42		
Yb		2.12	2.17		1.85			2.21	2.73		
Lu		0.31	0.32		0.29			0.36	0.43		
Hf		4.94	5.65		4.09			5.31	7.54		
Ta		1.28	1.38		1.32			1.21	1.47		
Th		21.3	20.8		26.4			21.3	21.2		
U		1.91	1.83		2.33			3.91	3.16		

[1]Fe_2O_3* = total iron.

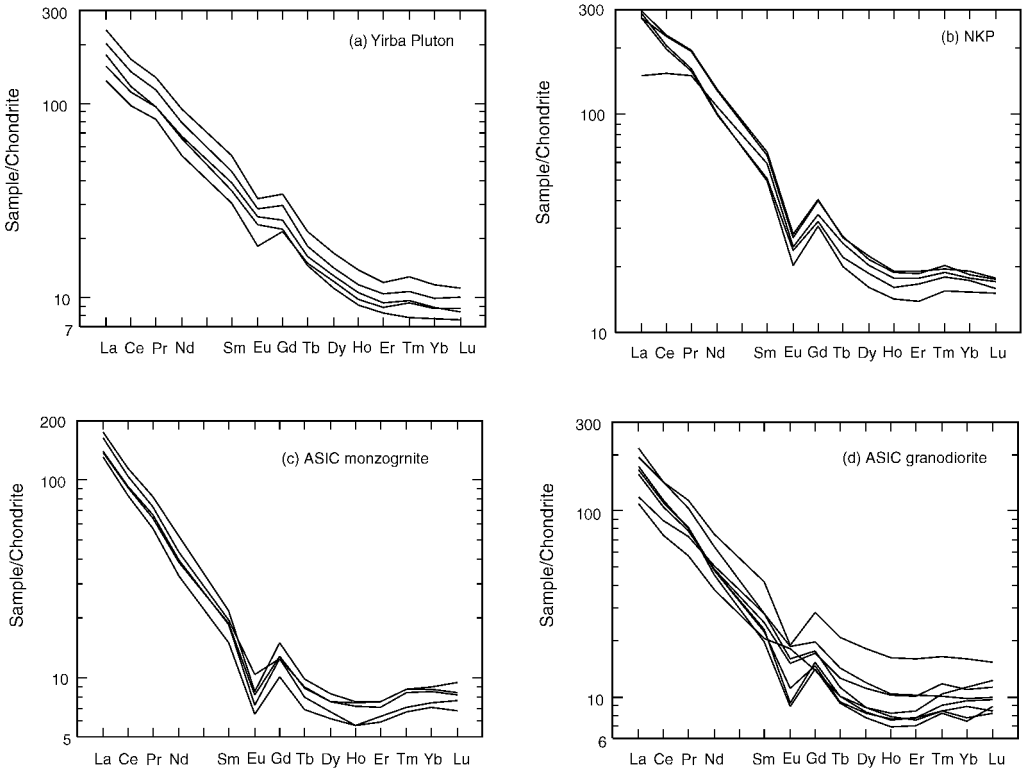

FIG. 5. Chondrite-normalized REE patterns for granitoids from the Kudi area.

Arkarz Shan intrusive complex

The granodiorite (212 ± 2 Ma) and monzogranite (215 ± 1 Ma) of the ASIC have indistinguishable ages, suggesting that they were produced in a single magmatic event. A 214 ± 1 Ma U-Pb age is obtained, when all the data are pooled. The ASIC is relatively LILE enriched and HFSE depleted, sharing features of volcanic-arc granites (Fig. 6); accordingly, it was previously considered to be generated by the subduction of Paleo-Tethys (e.g., Pan et al., 1994; Matte et al., 1996). However, we suggest that the ASIC intruded in a collisional environment, and its 214 Ma age well constrains the closure time of Paleo-Tethys in the West Kunlun, based on the following geological considerations. First, Upper Triassic red molasse beds unconformably overlie Permian shallow marine carbonates in the West Kunlun (Mattern and Schneider, 2000), suggesting that Paleo-Tethys was closed in the Late Triassic. Second, plant fossils were discovered in Upper Triassic strata, indicating a continental depositional environment (Pan, 1996). Third, granitoids of this age are widespread on both sides of the Paleo-Tethys suture (Yin and Bian, 1995; Matte et al., 1996; Xu et al., 1996; Zhang et al., 1996). This type of distribution is an important feature for collision-related granitoids (Sengör et al., 1991, 1993).

Tectonic Reconstruction

Consumption of Proto-Tethys

Juvenile Nd model ages (1.0–1.5 Ga) and the existence of ultramafic fragments in the metamorphic complex of the South Kunlun Block strongly suggest that the complex consists of accreted materials, rather than representing an Archean continental block rifted away from the Tarim Craton (Zhou, 1998; Li et al., 1999; Yuan, 1999). The 471 Ma Yirba pluton represents the earliest Paleozoic arc magmatism in the West Kunlun in relation to the consumption of Proto-Tethys. An intra-oceanic arc was developed in the Proto-Tethys probably at the same time, as indicated by the Yishake volcanic

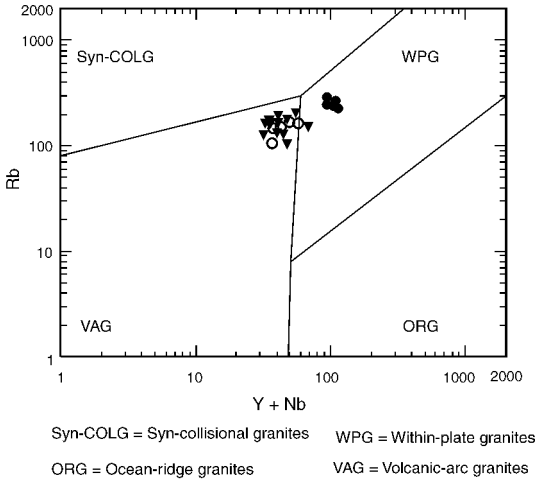

FIG. 6. Tectonic discrimination diagram for granitoids from the Kudi area (after Pearce et al., 1984) (symbols are the same as those used in Fig. 4).

sequence (Yuan, 1999) (Fig. 7A). As subduction continued, the intra-oceanic arc was accreted to the southern margin of the Tarim Craton, resulting in the first collisional event in the West Kunlun (Fig. 7B). The 451 to 380 Ma ^{40}Ar-^{39}Ar ages of various minerals from the metamorphic complex in the South Kunlun Block indicate that this collision occurred in the Middle Ordovician and perhaps continued to the Silurian, giving rise to the lack of Silurian strata in the West Kunlun (Pan et al., 1994).

Middle Paleozoic magmatic quiescence

The arc-continent collision ended in the Early Devonian, as indicated by the post-dynamic NKP and coeval lamprophyre dikes (Fig. 7C). Different opinions exist as to whether there was continuous subduction-related magmatism in the West Kunlun. The archipelago model envisages the West Kunlun as a magmatic front resulting from continuous northward subduction of Proto-and Paleo-Tethys from Late Precambrian to Early Mesozoic (Yao and Hsü, 1994; Hsü et al., 1995). However, recent geochronological investigation of selected granitoids in the West Kunlun showed that the granitoids intruded almost exclusively in the Early and Late Paleozoic, but rarely in the Middle Paleozoic (Xu et al., 1994, 1996). This led to a two-stage arc model for the Paleozoic evolution of the West Kunlun (Pan et al., 1994; Pan, 1996), although the cause of the magmatic quiescence was unclear. Based on analysis of the sedimentary sequence, Yin and Harrison (2000) proposed an extensional scheme to explain the absence of Devonian to Early Permian magmatism in the West Kunlun. The existence of the NKP and coeval lamprophyre dikes strongly support the two-stage arc model by indicating an extensional environment in the West Kunlun. In the East Kunlun, analysis of sedimentary facies indicated a similar extensional setting between the Devonian and Permian (Chang et al., 1986; Gu et al., 1996; Xu et al., 1998). A similar lack of Middle Paleozoic magmatism was noted in the North Pamir (Debon et al., 1987), and recent $^{40}Ar/^{39}Ar$ work on basement rocks of the East Kunlun also revealed an age gap between 360 Ma and 240 Ma (Liu et al., 2000). These geological and geochronological data suggest that the magmatic quiescence persisted for about 100 m.y. throughout the Kunlun orogenic belt.

Suturing of Paleo-Tethys

Paleo-Tethys started to consume in the Early Permian, as manifested by Permian arc volcanic rocks in the South Kunlun Block (Chang et al., 1989; Pan et al., 1994; Wang, 1996) (Figs. 2 and 7D). Subduction ceased in the Late Triassic due to the final closure of Paleo-Tethys, as indicated by molasse deposits and sediments with plant fossils in the West Kunlun (Pan et al., 1994; Mattern and Schneider, 2000). During such a collision, shortening and thickening of the crust might have led to delamination of the eclogitized crustal root, upwelling of asthenospheric mantle, and an increase

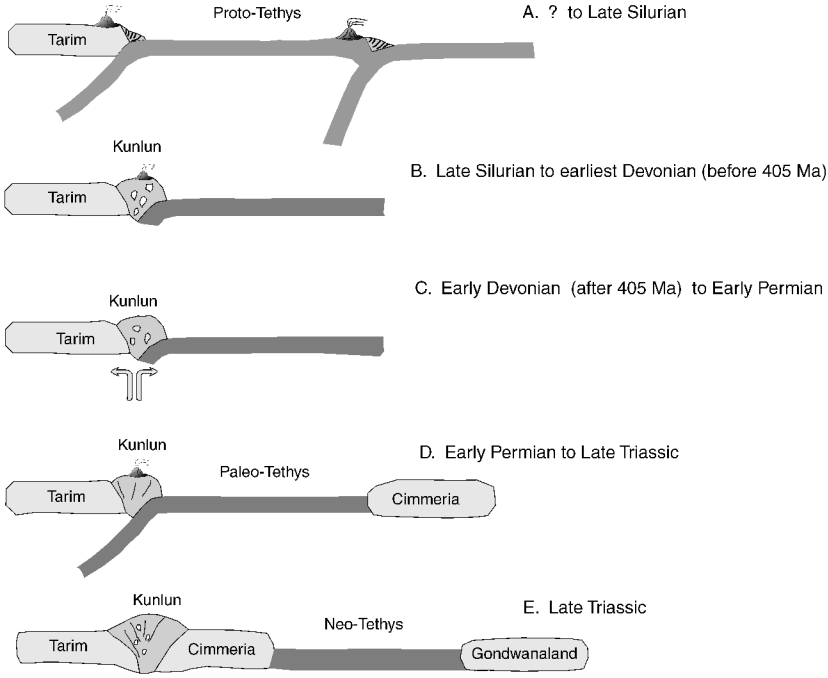

FIG. 7. Schematic diagram for tectonic evolution of the West Kunlun.

in heat input (Costa and Rey, 1995). This could have caused melting of the crustal material to generate abundant collision-related granitic intrusions (Stern et al., 1994; Förster et al., 1997) on both sides of the Paleo-Tethys suture (Fig. 7E). The voluminous ASIC has consistent zircon U-Pb (214 Ma) and biotite $^{40}Ar/^{39}Ar$ (213 Ma) ages, indicating rapid cooling/uplifting rates, and therefore a post-collisional environment.

Conclusions

The Yirba pluton possesses characteristics typical of volcanic-arc granites and was intruded in the Early Ordovician (471 ± 5 Ma) in the active southern margin of the Tarim craton, representing an early product of Proto-Tethys consumption. The North Kudi pluton, dated at 405 ± 2 Ma, displays a strong affinity to A-type granites. Its post-kinematic characteristics imply that an extensional tectonic environment that may be responsible for the Devonian to Early Permian magmatic quiescence in the Kunlun orogenic belt. The Arkarz Shan intrusive complex was emplaced in a rapid uplifting environment corresponding to the closure of Paleo-Tethys during the Late Triassic (214 ± 1 Ma).

Acknowledgments

We are grateful to Professors Zhang Yuquan, Pan Yusheng, and Xu Ronghua for enlightening discussions, and to Drs. Hou Quanlin, Wang Zhihong, Chen Hanlin, Zhang Guocheng, and Fang Aimin for their cordial cooperation in the field in 1996. Special thanks are given to An Yin, Paul Kapp, Eric Cowgill, Brian Windley, Guochun Zhao, and Paul Robinson for their constructive suggestions and assistance in polishing the English. This research was supported by Chinese Project 973 (2001CB409801), the National Science Foundation of China (project 40003005), a grant from the University of Hong Kong (335/029/0012), and grants from Ministry of Education and the Chinese Academy of Sciences. A postgraduate stipend from HKU to Chao Yuan is gratefully acknowledged.

REFERENCES

Arnaud, N., 1992, The cooling history of western Kunlun and central Tibet and its bearing on India-Asia collision tectonics, *in* International Symposium on the Karakorum and Kunlun Mountains, Kashi, China, p. 53.

Arnaud, N., and Vidal, Ph., 1990, Geochronology and geochemistry of the magmatic rocks from the Kunlun-Karakorum geotraverse, *in* Colloque Kunlun-Karakorum: Paris, France, IGP, p. 52,

Barbarin, B., 1999, A review of the relationships between granitoid types, their origins and their geodynamic environments: Lithos, Vol. 46, p. 605–626.

Chang, C. F., Pan, Y. S., and Sun, Y. Y., 1989, The tectonic evolution of the Qinghai-Tibet plateau: A review, *in* Sengör, A. M. C., ed., Tectonic evolution of the Tethyan regions: Dordrecht, Netherlands, Reidel, p. 415–476.

Chang, C., Chen, N., Coward, M. P., Deng, W., Dewey, J. F., Gansser, A., Harris, B. W., Kidd, W. S. F., Leeder, M. R., Li, H., Lin, J., Liu, C., Mei, H., Molnar, P. Pan, Y., Pearce, J. A., Shackleton, R. M., Smith, A. B., Sun, Y., Ward, M., Watts, D. R., Xu, J., Xu, R., Yin, J., and Zhang, Y., 1986, Preliminary conclusions of the Royal Society and Academia Sinica 1985 geotraverse of Tibet: Nature, Vol. 323, p. 501–507.

Christiansen, E. H., and Keith, J. D., 1996, Trace element systematics in silicic magmas: A metallogenic perspective, *in* Wyman, D. A., ed., Trace element geochemistry of volcanic rocks: Applications for massive sulphide exploration: Geological Association of Canada Short Course Notes, v. 12.

Costa, S., and Rey, P., 1995, Lower crustal rejuvenation and growth during post-thickening collapse; insights from a crustal cross section through a Variscan metamorphic core complex: Geology, v. 23, p. 905–908.

Debon, F., Afzali, H., Le Fort, P. and Sonet, J., 1987, Major intrusive stages in Afghanistan: Typology, age, and geodynamic setting: Geologische Rundschau, v. 76, p. 245–264.

Defant, M. J., and Drummond, M. S., 1990, Derivation of some modern arc magmas by melting of young subducted lithosphere: Nature, v. 347, p. 663–665.

Deng, W., 1995, Geological features of ophiolite and tectonic significance in the Karakorum West Kunlun Mts.: Acta Petrologica Sinica, v. 11, suppl. p. 98–111 (in Chinese with English abs.).

Dewey, J. F., Shackleton, R. M., Chang, C. F., and Sun, Y. Y., 1988, The tectonic evolution of Tibetan Plateau: Philosophical Transactions of the Royal Socicty of London, v. 327, p. 379–413.

Ding, D., Wang, D., Liu, W., and Sun, S., 1996, The Western Kunlun orogenic belt and basin: Beijing, China, Geological Publishing House (in Chinese, with English summary).

Eby, G. N., 1992, Chemical subdivision of the A-type granitoids: Petrogenetic and tectonic implications: Geology, v. 20, p. 641–644.

Fang, A., Li, J., Hou, Q., Zhou, H., Wan, S., and Li, H., 1998, The first discovery of radiolarian fossils in Yishakegou flesch section of Kuda, West Kunlun, China: Scientia Geologica Sinica, v. 33, p. 300.

Förster, H.-J., Tischendorf, G., and Trumbull R. B., 1997, An evaluation of the Rb vs. (Y+Nb) discrimination diagram to infer tectonic setting of silicic igneous rocks: Lithos, v. 40, p. 261–293.

Gaetani, M., Gosso, G., and Pognante, U., 1990, A geological transect from Kunlun to Karakorum (Sinkiang, China): The western termination of the Tibetan Plateau. Preliminary note: Terra Nova, v. 2, p. 23–30.

GITT (Geological Investigation Team Two, Bureau of Geology and Mineral Resources of Xinjiang Uygur Autonomous Region), 1985, Geological map of Southwest Xinjiang (1:500,000) and explanation: Beijing, China: Geological Press.

Goto, A., and Tatsumi, Y., 1996, Quantitative analyses of rock samples by X-ray fluorescence spectrometer (I): The Rigaku Journal, v. 11, p. 40–59.

Gu, F., Wu, X., and Jiang, C., 1996, Assemblages and tectonic environment of Variscan-Indosinian granitoid in the Eastern Kunlun: Qinghai Geology, no. 1, p. 18–36 (in Chinese with English abstract).

Hsü, K. J., Pan, G., Sengör, A. M. C., Briegel, U., Chen, H., Chen, C., Harris, N., Hsü, P., Li, J., Luo, J., Lee, T., Li, Z., Lu, C., Powell, C., Wang, Q., and Winterer, E. L., 1995, Tectonic evolution of the Tibetan Plateau: A working hypothesis based on the archipelago model of orogenesis: International Geology Review, v. 37, p. 473–508.

Le Maitre, R. W., 1989, A classification of igneous rocks and glossary terms: Recommendations of the International Union of Geological Sciences Submissions on the systematics of igneous rocks: Oxford, UK, Blackwell.

Li, J., Niu, B., Liu, Z., and Qu, G., 2000, Tectonic deformation and major tectonothermal events of the Central Orogenic Belt, *in* Jiang, C., Wang, Z. and Li, J., eds, Opening–closure tectonics of the Central orogenic belt: Beijing, China: Geological Publication House, p. 104–134 (in Chinese with English abstract).

Li, J., Sun, S., Hao, J., Chen, H., Hou, Q., and Xiao, W., 1999, On the classification of collision orogenic belts: Scientia Geologica Sinica, v. 34, p. 129–138 (in Chinese with English abstract).

Li, Y., Li, X., Sun, D., and Han, Y., 1995, Tectonic evolution of Qiangtang block and Kangxiwar structure zone in Kara-Kunlun Shan southwest of Xinjiang, China: Urumuqi, China, Xinjiang Science and Technology and Hygiene Publishing House (in Chinese with English summary).

Liu, Y., Jenser, G., Franz, N., Jin, W., Ge, X., and Robert, H., 2000, Geochronology of $^{40}Ar/^{39}Ar$ dating in the basement rocks in East Kunlun Shan and its tectonic implications [abs.]: Earth Science Frontiers, v. 7, Suppl. (Abs. volume of 15th HKT workshop), p. 227.

Liu, Y., Liu, H., and Li, X., 1996, Simultaneous and precise determination of 40 trace elements in rock samples using ICP-MS: Geochimica, v. 25, p. 552–558 (in Chinese with English abstract).

Ludwig, K. R., 1998, ISOPLOT: A plotting and regression program for radiogenic-isotope data; version 2.96: U. S. Geological Survey Open-File Report 91–445.

Matte, Ph., Tapponnier, P., Arnaud, N., Bourjot, L., Avouac, J. P., Vidal, Ph., Liu Q., Pan Y., and Wang Y., 1996, Tectonics of Western Tibet, between the Tarim and the Indus: Earth and Planetary Science Letters, v. 142, p. 311–330.

Mattern, F., and Schneider, W., 2000, Suturing of the Proto-and Paleo-Tethys oceans in the western Kunlun (Xinjiang, China): Journal of Asian Earth Sciences, v. 18, p. 637–650.

Mattern, F., Schneider, W., Li, Y., and Li, X., 1996, A traverse through the western Kunlun (Xinjiang, China): Tentative geodynamic implications for the Paleozoic and Mesozoic: Geologische Rundschau, v. 85, p. 705–722.

Pan Y., 1996, Regional geological evolution and conclusion, *in* Pan, Y., ed., Geological evolution of the Karakorum and Kunlun Shan: Beijing, China, Seismological Press, p. 263–288.

Pan, Y. and Bian, Q., 1996. Tectonics, *in* Pan, Y., ed.,, Geological evolution of the Karakorum and Kunlun Shan: Beijing, China, Seismological Press, p. 230–262.

Pan, Y., Wang, Y., Matte, Ph., and Tapponnier P., 1994, Tectonic evolution along the geotraverse from Yecheng to Shiquanhe: Acta Geologica Sinica, v. 68, p. 295–307.

Pearce, J. A., Harris, N. B. W., and Tindle, A. G., 1984, Trace element discrimination diagram for the tectonic interpretation of granitic rocks: Journal of Petrology, v. 25, p. 956–983.

Pitcher, W. S., 1993, The nature and origin of granite: Glasgow, UK, Blackie Academic and Professional.

Sengör, A. M. C., Cin A., Rowley D. B., and Nie, S-Y., 1991, Magmatic evolution of the Tethysides: A guide to reconstruction of collage history: Palaeogeography, Palaeoclimatology, Palaeoecology, v. 87, p. 411–440.

_____, 1993, Space-time patterns of magmatism along the Tethysides: A preliminary study: Journal of Geology, v. 101, p. 51–84.

Stacey, J. S., and Kramers, J. D., 1975, Approximation of terrestrial lead isotope evolution by a two-stage model: Earth and Planetary Science Letters, v. 26, p. 207–221.

Stern, G., Charvet, J., Lapierre, H., and Fabbri, O., 1994. Geodynamic setting of volcano-plutonic rocks in so-called "paleo-accretionary prism": Fore-arc activity or post-collisional magmatism? The Shimanto belt as a case study: Lithos, v. 33, p. 85–107.

Wang, T., 1996, Characteristics of sedimentary rocks and their environmental evolution, *in* Pan, Y., ed., Geological evolution of the Karakorum and Kunlun mountains: Beijing, China, Seismological Press, p. 22–50.

Wang, Y., and Fang, X., 1987, Preliminary discussion on the temporal and spatial distribution of granitoids in the West Kunlun and Karakorum: Xinjiang Geology, v. 5, p. 9–24.

Wang, Y., Qian, Q., and Zhang, Q., 2000, Geochemical characteristics and tectonic implications of adakite: Scientia Geologica Acta, v. 35, p. 251–256.

Wang, Z. H., Hou, Q. L., Li, J. L., and Chen, H. H., 2000, Platinum group elements study for Kudi ophiolite, Western Kunlun: Chinese Science Bulletin, v. 45, p. 551–556.

XBGMR (Xinjiang Bureau of Geology and Mineral Resource), 1985, Explanatory notes on the Geological map of Xinjiang Uygur Autonomous Region, China (1:2,000,000): Beijing, China, Geological Publication House.

Xiao, W., Windley, B. F., Hao, J. and Li, J., 2002, Arc-ophiolite obduction in the western Kunlun range (China): Implications for the Paleozoic evolution of central Asia: Journal of the Geological Society of London (in press).

Xu, Q., Pan, G., Xu, Z., and Yang, J., 1998, Evolution of the sedimentary environments and basins in East Kunlun during Late Paleozoic to Triassic time: Tethyan Geology, no. 22, p. 76–89. (in Chinese with English abstract)

Xu, R., Zhang, Y., Vidal, Ph., and Arnaud, N., 1992, Two plutonic belts in western Kunlun, *in* International Symposium on the Karakorum and Kunlun Mountains, Kashi, China, p. 62.

Xu, R., Zhang, Y., Xie, Y., Chen, F., Vidal, Ph., Arnaud, N., Zhang, Q., and Zhao, D., 1994, A discovery of an early Palaeozoic tectono-magmatic belt in the Northern part of west Kunlun Shan: Scientia Geologica Sinica, v. 29, p. 313–328.

Xu, R., Zhang, Y., Xie, Y., Vidal, Ph., Arnaud, N., Zhang, Q., and Zhao, D., 1996, Isotopic geochemistry of plutonic rocks, *in* Pan, Y., ed., Geological evolution of the Karakorum and Kunlun Shan: Beijing, China, Seismological Press, p. 137–186.

Yang, J. S., Robinson, R. T., Jiang, C. F., and Xu, Z. Q., 1996, Ophiolites of the Kunlun Shan, China and their tectonic implications: Tectonophysics, v. 258, p. 215–231.

Yao, Y., and Hsü, K. J., 1994, Origin of the Kunlun Shan by arc-arc and arc-continent collisions: The Island Arc, v. 3, p. 75–89.

Yin, A., and Harrison, T. M., 2000, Geologic evolution of the Himalayan-Tibetan Orogen: Annual Review of Earth and Planetary Sciences, v. 28, p. 211–280.

Yin, J. X., and Bian, Q. T., 1995, Geological map of the Karakorum—West Kunlun and adjacent regions (1:2,000,000). Beijing, China, Science Press.

Yuan, C., 1999, Magmatism and tectonic evolution of the West Kunlun Mountains: Unpubl. Ph.D. thesis, University of Hong Kong.

Yuan, C., Sun, M., Zhou, M. F., Hou, Z., Xiao, W. J., and Li, J. L., 2002, Absence of Archean basement in the South Kunlun block: Nd-Sr-O isotopic evidence from granitoids: The Island Arc (in press).

Zhang, Y., Xie, Y., Xu, R., Vidal, Ph., and Arnaud, N., 1996, Geochemistry of granitoid rocks, *in* Pan, Y., eds., Geological evolution of the Karakorum and Kunlun Shan: Beijing, China, Seismological Press, p. 94–136.

Zhang, Y., Zhu, B., Xie, Y., Harrison, T. M., and Kidd, S. F., 1998, The uplifting rates for the Western Qinhai-Xizang Plateau: granites in the area from Yecheng to Shiquanhe: Acta Petrologica Sinica, v. 14, p. 11–21.

Zhou, H., 1998, The main ductile shear zone and the lithosphere effective elastic thickness of west Kunlun orogenic belt: Unpubl. Ph. D thesis, Institute of Geology, Chinese Academy of Sciences, Beijing, China (in Chinese with English abstract).

Zhou, H., Chu, Z., Li, J., Hou, Q., Wang, Z., and Fang, A., 2000, $^{40}Ar/^{39}Ar$ dating of the ductile shear zone in Kuda, West Kunlun, Xinjiang: Scientia Geologica Sinica, v. 35, p. 233–239 (in Chinese with English abstract).

Zhou, H., and Li, J., 2000, Age and geochemical features of lamprophyres in Kuda, western Kunlun: Acta Petrologica Sinica, v. 16, p. 380–384 (in Chinese with English abstract).

Zhou, H., Li, J., Hou, Q., Fang, A., and Li, H., 1998, The recognition and implications of the early Paleozoic radiolarian fossils of Kuda melange: Chinese Science Bulletin, v. 43, p. 2448–2450 (in Chinese).